AD-A108 483 MICHIGAN UNIV ANN ARBOR ELECTRON PHYSICS LAB F/G 9/5
SIMULATION OF PULSED IMPATT OSCILLATORS AND INJECTION-LOCKED AM--ETC(U)
OCT 81 R K MAINS, G I HADDAD, D F PETERSON F33615-77-C-1132
UNCLASSIFIED TR-151 AFWAL-TR-81-1177 NL

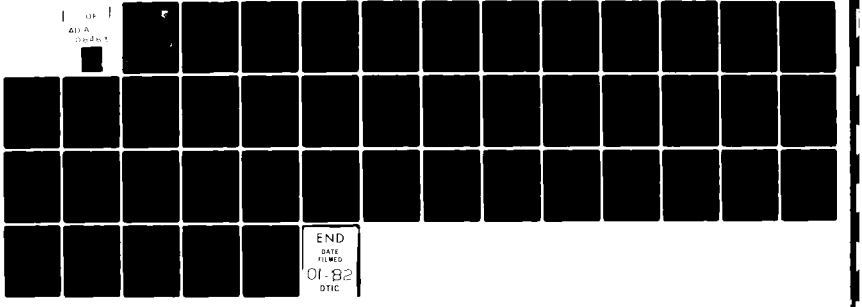

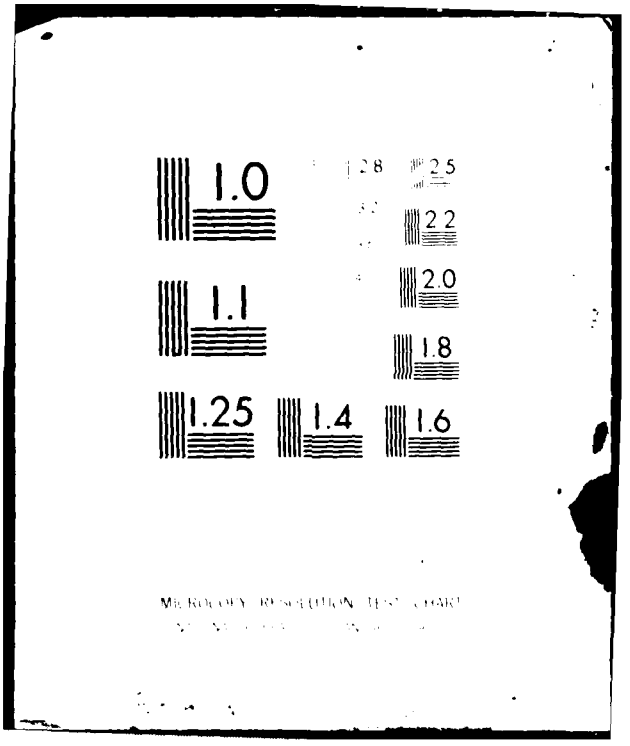
1.0
1.1
1.25
1.4
1.6
2.0
1.8
2.2
2.5

AFWAL-TR-81-1177

SIMULATION OF PULSED IMPATT OSCILLATORS AND INJECTION-LOCKED AMPLIFIERS

R. K. MAINS
G. I. HADDAD
D. F. PETERSON

ELECTRON PHYSICS LABORATORY
DEPARTMENT OF ELECTRICAL AND COMPUTER ENGINEERING
THE UNIVERSITY OF MICHIGAN
ANN ARBOR, MICHIGAN 48109

OCTOBER 1981

TECHNICAL REPORT AFWAL-TR-81-1177
Interim Report for Period June 1980 — February 1981

Approved for public release; distribution unlimited

AVIONICS LABORATORY
AIR FORCE WRIGHT AERONAUTICAL LABORATORIES
AIR FORCE SYSTEMS COMMAND
WRIGHT-PATTERSON AIR FORCE BASE, OHIO 45433

NOTICE

When Government drawings, specifications, or other data are used for any purpose other than in connection with a definitely related Government procurement operation, the United States Government thereby incurs no responsibility nor any obligation whatsoever; and the fact that the government may have formulated, furnished, or in any way supplied the said drawings, specifications, or other data, is not to be regarded by implication or otherwise as in any manner licensing the holder or any other person or corporation, or conveying any rights or permission to manufacture use, or sell any patented invention that may in any way be related thereto.

This report has been reviewed by the Office of Public Affairs (ASD/PA) and is releasable to the National Technical Information Service (NTIS). At NTIS, it will be available to the general public, including foreign nations.

This technical report has been reviewed and is approved for publication.

JON E. GRIGUS, CAPT, USAF
Project Engineer
Microwave Techniques &
Applications Gp

ALAN R MERTZ, CAPT, USAF
Chief, Microwave Techniques &
Applications Gp
Avionics Laboratory

FOR THE COMMANDER

DONALD S. REES, Chief
Microwave Technology Branch
Avionics Laboratory

"If your address has changed, if you wish to be removed from our mailing list, or if the addressee is no longer employed by your organization please notify AFWAL/AADM, W-PAFB, OH 45433 to help us maintain a current mailing list."

Copies of this report should not be returned unless return is required by security considerations, contractual obligations, or notice on a specific document.

AIR FORCE/56780/24 November 1981 — 210

Unclassified

SECURITY CLASSIFICATION OF THIS PAGE *(When Data Entered)*

REPORT DOCUMENTATION PAGE	READ INSTRUCTIONS BEFORE COMPLETING FORM
1. REPORT NUMBER: AFWAL-TR-81-1177	2. GOVT ACCESSION NO.: AD-A108483
3. RECIPIENT'S CATALOG NUMBER	
4. TITLE *(and Subtitle)*: SIMULATION OF PULSED IMPATT OSCILLATORS AND INJECTION-LOCKED AMPLIFIERS	5. TYPE OF REPORT & PERIOD COVERED: Interim, June 1980-February 1981
	6. PERFORMING ORG. REPORT NUMBER: Tech. Report No. 151
7. AUTHOR(s): R. K. Mains, G. I. Haddad and D. F. Peterson	8. CONTRACT OR GRANT NUMBER(s): F33615-77-C-1132
9. PERFORMING ORGANIZATION NAME AND ADDRESS: Electron Physics Laboratory, The University of Michigan, Ann Arbor, MI 48109	10. PROGRAM ELEMENT, PROJECT, TASK AREA & WORK UNIT NUMBERS: 20020351
11. CONTROLLING OFFICE NAME AND ADDRESS: Avionics Laboratory (AFWAL/AADM-2), Air Force Wright Aeronautical Laboratories (AFSC), Air Force Systems Command, WPAFB, OH 45433	12. REPORT DATE: October 1981
	13. NUMBER OF PAGES: 38
14. MONITORING AGENCY NAME & ADDRESS *(if different from Controlling Office)*	15. SECURITY CLASS. *(of this report)*: Unclassified
	15a. DECLASSIFICATION/DOWNGRADING SCHEDULE: N/A

16. DISTRIBUTION STATEMENT *(of this Report)*

Approved for public release; distribution unlimited.

17. DISTRIBUTION STATEMENT *(of the abstract entered in Block 20, if different from Report)*

18. SUPPLEMENTARY NOTES

The findings in this report are not to be construed as an official Department of the Air Force position, unless so designated by other authorized documents.

19. KEY WORDS *(Continue on reverse side if necessary and identify by block number)*

Pulsed IMPATT oscillators and amplifiers
Quasi-static approximation
Device-circuit interaction
High-Low GaAs IMPATT
Double-drift structures

20. ABSTRACT *(Continue on reverse side if necessary and identify by block number)*

A method for simulating the dynamic behavior of pulsed IMPATT oscillators using a quasi-static approximation is presented. The method used to characterize the IMPATT diode is explained. A particular circuit model is used which models the cylindrical cavity power combining circuit. The overall device-circuit interaction technique is outlined. Simulation results for a high-low, single-drift X-band GaAs IMPATT are presented. The method presented here can be employed for any type of IMPATT device. The pulsed oscillator properties of double-drift IMPATT diode structures are presently being investigated.

DD FORM 1 JAN 73 1473

Unclassified

SECURITY CLASSIFICATION OF THIS PAGE *(When Data Entered)*

FOREWORD

This report describes the simulation of pulsed IMPATT oscillators and injection-locked amplifiers at the Electron Physics Laboratory, Department of Electrical and Computer Engineering, The University of Michigan, Ann Arbor, Michigan. The work was sponsored by the Air Force Systems Command, Air Force Avionics Laboratory, Wright-Patterson Air Force Base, Ohio under Contract No. F33615-77-C-1132.

The work reported herein was performed during the period June 1980 to February 1981 by Drs. R. K. Mains, G. I. Haddad and D. F. Peterson. The report was released by the authors in July 1981.

The authors wish to thank Captains Jon Grigus and Alan Mertz for their insightful comments and suggestions concerning this work.

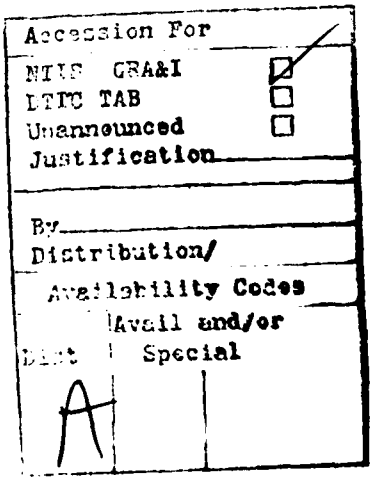

TABLE OF CONTENTS

LIST OF ILLUSTRATIONS

Introduction

This report presents a method of simulating the dynamic behavior of pulsed IMPATT oscillators and amplifiers. The problem is greatly simplified by using the quasi-static approximation, which assumes that the quantities of interest are changing slowly with respect to the RF period. Although full device-circuit interaction simulations can be performed to study pulsed IMPATT behavior, such simulations are costly and it is difficult to incorporate dynamic temperature effects.

The basic theory of the quasi-static approach is presented first. The application of the theory to the cylindrical resonant cavity power combining circuit is then outlined. The method of characterizing the IMPATT diode structures is explained and the overall device-circuit interaction simulation procedure is outlined. Simulation results using a high-low GaAs IMPATT operating at 10 GHz are presented. The procedure outlined here can also be employed to determine the properties of other doping profiles and double-drift structures. Such studies are presently being carried out.

The Quasi-Static Approximation Model

In steady-state ac circuit theory, the differential equation is converted to a phasor equation by replacing the time derivative by the factor $j\omega$. For this case, the amplitudes and phases of the circuit voltages and currents are constant with time.

The quasi-static approximation assumes that the amplitudes and phases of the circuit response vary slowly in time and thus the change is negligible during the period of the RF signals.[1] Therefore, a circuit voltage would have the form:

$$v(t) = \mathrm{Re}\left\{V(t)e^{j[\omega_o t + \phi(t)]}\right\} \quad . \tag{1}$$

Differentiating Equation 1 with respect to time yields:

$$\frac{dv(t)}{dt} = \mathrm{Re}\left\{\left[\frac{1}{V(t)}\frac{dV(t)}{dt} + j\left[\omega_o + \frac{d\phi(t)}{dt}\right]\right]V(t)e^{j[\omega_o t + \phi(t)]}\right\} \quad . \tag{2}$$

From Equation 2 it is seen that the time derivative in phasor space using the quasi-static approximation is obtained from multiplication by the complex frequency $s = \sigma + j\omega$, where

$$\sigma = \frac{1}{V(t)}\frac{dV(t)}{dt} \tag{3}$$

and

$$\omega = \omega_o + \frac{d\phi(t)}{dt} \quad . \tag{4}$$

Equations 3 and 4 may be used as follows. It is assumed that a circuit response voltage is in a particular state at time t, that is with a given $V(t)$ and $\phi(t)$. Given this particular state, there is a unique value of complex frequency s that solves the circuit equations in phasor space. Once this value of s is obtained, Equations 3 and 4 predict how the circuit voltage amplitude and phase will change with time. A time step advancement Δt is taken using Equations 3 and 4 to calculate $V(t + \Delta t)$ and $\phi(t + \Delta t)$. For this new amplitude and phase the circuit equations are solved for a new complex frequency s and the process is repeated. In this way the time evolution of $V(t)$ and $\phi(t)$ in Equation 1 is determined.

Application to IMPATT Diodes in a Cylindrical Resonant Cavity Circuit

An IMPATT circuit which is currently of much interest is the cylindrical resonant cavity.[2] This circuit is used to combine the output of several IMPATT diodes. The circuit is illustrated in Figure 1, where Figure 1a shows the coupling between one coaxial module and the cavity and Figure 1b shows how several modules are combined.

In this analysis, the interactions between diode modules are not included; rather, a single module as in Figure 1a is simulated, assuming a particular model for the resonant cavity. Figure 2 shows the complete equivalent circuit model attached to the IMPATT diode terminals at plane D. R_s, L_s and C_p are the package-mounting parasitics. For all simulations in this report, the values $R_s = 0.25\ \Omega$, $L_s = 0.24$ nH and $C_p = 0.32$ pF were used (these L_s, C_p values are for an X-band package used by Microwave Associates, Inc.). The first transmission-line section, characterized by length l_1 and impedance Z_1, models the quarter-wave transformer shown in Figure 1a. This transformer matches the relatively high impedance at the cavity to the low impedance at the diode terminals. The next transmission-line section in Figure 2 corresponds to the half-wavelength coaxial line in Figure 1a between the transformer and the resonant cavity. Since the frequency of operation wanders during the simulation, these sections are not always $\lambda/4$ and $\lambda/2$ long; for this reason the transmission lines are included in the circuit model. If the frequency were constant, a simple impedance inverter would adequately model the coaxial sections in Figure 1a.

In Figure 1a it is seen that the cavity is in series with a matched terminating resistor; this resistor is R in Figure 2 and

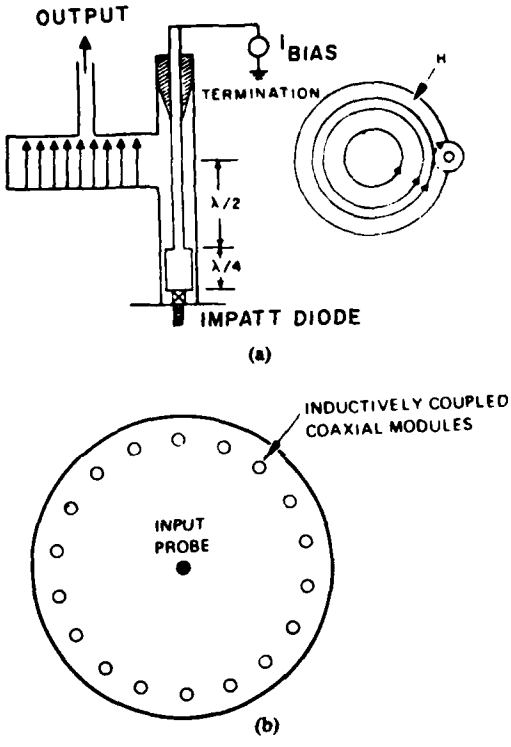

FIG. 1 CYLINDRICAL RESONANT CAVITY COMBINER. (a) A SINGLE COAXIAL CIRCUIT MODULE ILLUSTRATING MAGNETIC COUPLING TO TM_{010} CAVITY. (b) TOP VIEW OF RESONANT CAVITY SHOWING MODULE POSITIONS AROUND PERIPHERY. (RUSSELL[2])

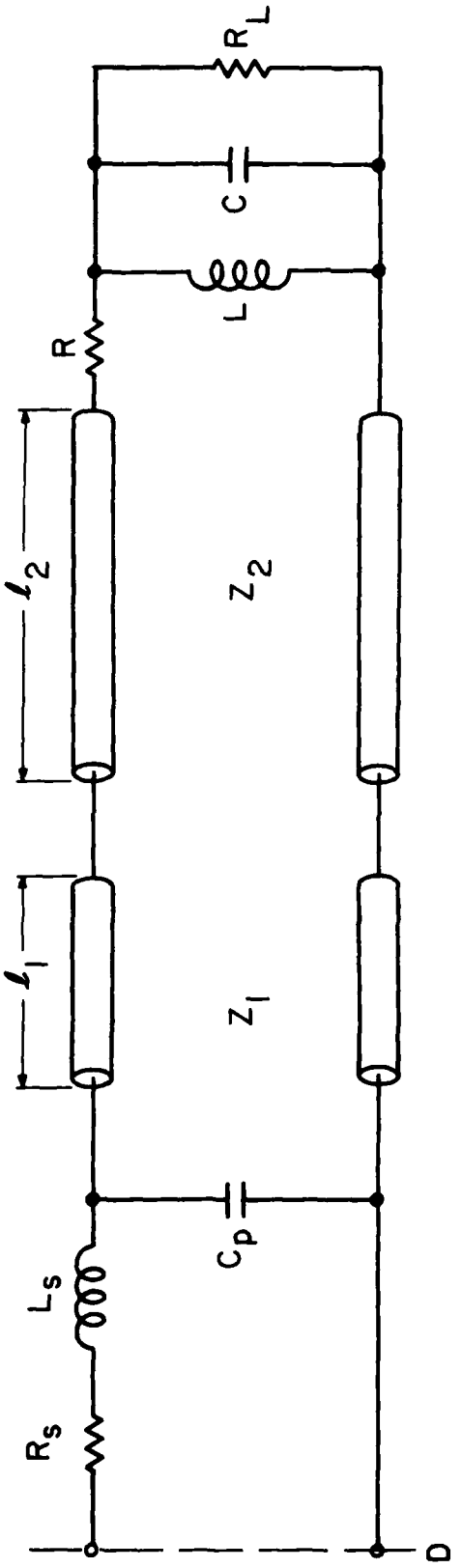

FIG. 2 EQUIVALENT CIRCUIT MODEL AS SEEN AT THE DIODE TERMINALS (PLANE D).

is set to 50 Ω for all the simulations. The cavity itself is modeled as a parallel RLC resonant circuit. At resonance, the cavity appears as a large real impedance, given by R_L in Figure 2; for the simulations in this report, R_L = 500 Ω was used. L and C are chosen to set the desired resonant frequency of the cavity as well as the cavity Q. For these simulations, a constant value L = 0.396×10^{-10} h was used and the capacitance C was varied. This sets the cavity Q at 200 for operation near 10 GHz. C must be chosen so that the cavity resonant frequency is near the desired operating frequency, however, the two need not be exactly equal. In these simulations, it was found advantageous to set the cavity resonant frequency at f_o = 9.98 GHz for 10-GHz operation. If this is done, the RF voltage can build up at a lower temperature and therefore sooner after the bias pulse is turned on. Varying the capacitance C in Figure 2 corresponds to physically tuning the cavity by changing the probe position, which is actually done experimentally to optimize the performance.

To carry out the simulation, the program must calculate the circuit input admittance at plane D in Figure 2 for any complex frequency s, denoted by $Y_c(s)$. Also, the derivative of this admittance, or $dY_c(s)/ds$, must be calculated for use in a Newton search algorithm.

Method of Characterizing the IMPATT Diode

In addition to the circuit admittance functions $Y_c(s)$ and $dY_c(s)/ds$, the program requires a large-signal characterization of the IMPATT diode. The finite-difference program developed at the Electron Physics Laboratory and described in a previous report[3] was used to calculate this information. The structure simulated in this report is a high-low, single-drift GaAs IMPATT structure whose doping profile

is shown in Figure 3. The information required is the diode admittance and the dc voltage as a function of RF voltage, dc current density, and device temperature.

An important assumption is made at this point. Since the circuit Q is very high, the frequency of operation will be close to the resonant frequency of the cavity throughout the simulation. For this reason it is assumed sufficient to characterize the diode only at the steady-state operating frequency of 10 GHz. This is a reasonable assumption since the diode properties do not vary much for frequencies close to the operating frequency.

Large-signal simulations for the structure of Figure 3 were carried out at the following temperatures: 300, 400, 500, 535 and 575°K. For each temperature, simulations were carried out for three current densities: J_{dc} = 1000, 1250 and 1500 A/cm^2. This represents 15 sets of simulations. Within each set, i.e., for each combination of temperature and J_{dc}, large-signal runs were performed over a range of RF voltages from small signal to a point beyond the RF voltage for which maximum efficiency was obtained. Also, a diode model for J_{dc} = 0 was included consisting of the cold capacitance in series with a small resistance to model the undepleted region of the diode.

These data were tabulated and read into the device-circuit interaction program. This provides the program with $Y_D(V_{RF},J_{dc},T)$ and $V_{dc}(V_{RF},J_{dc},T)$ for discrete values of V_{RF}, J_{dc} and T. Since the program requires knowledge of Y_D and V_{dc} for any values of V_{RF}, J_{dc} and T, an interpolation scheme must be used between tabulated values.

Figure 4 shows the large-signal results obtained for the high-low structure at J_{dc} = 1250 A/cm^2 for two temperatures:

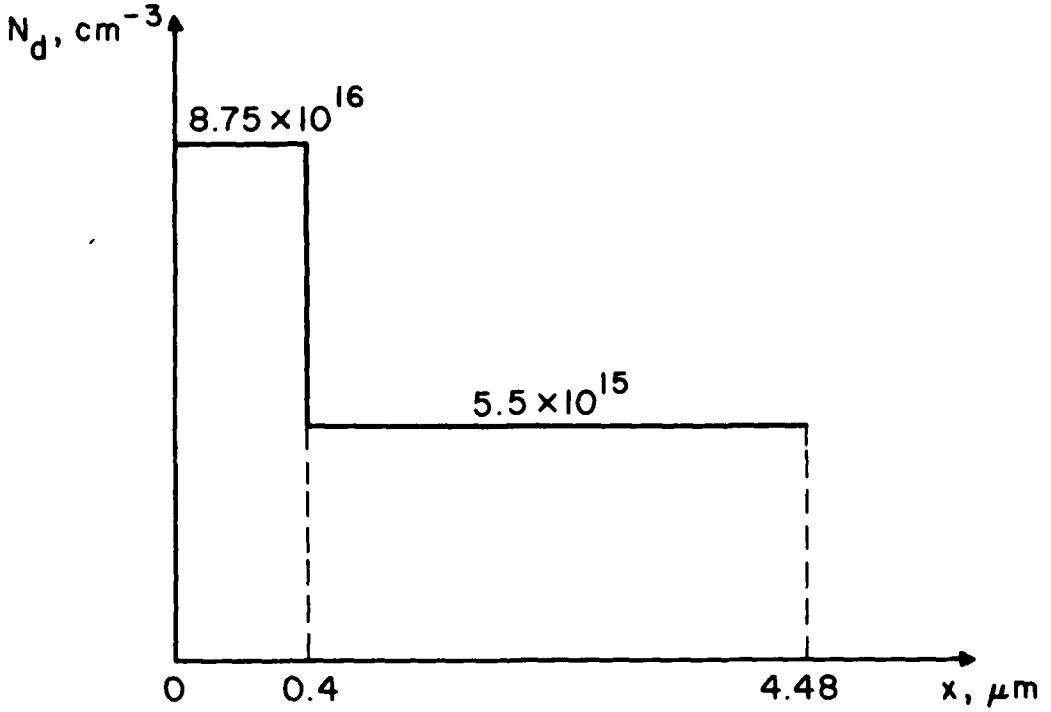

FIG. 3 DOPING PROFILE OF THE GaAs IMPATT DIODE SIMULATED IN THIS REPORT.

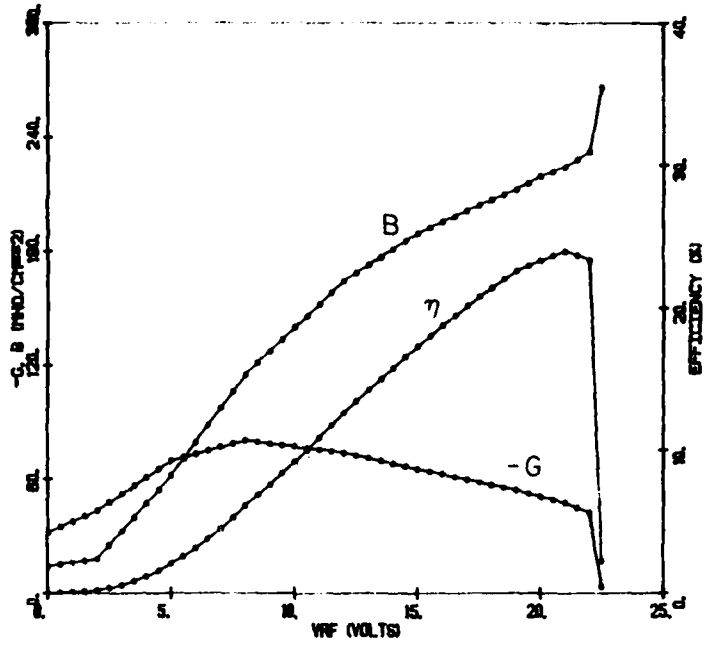

(a)

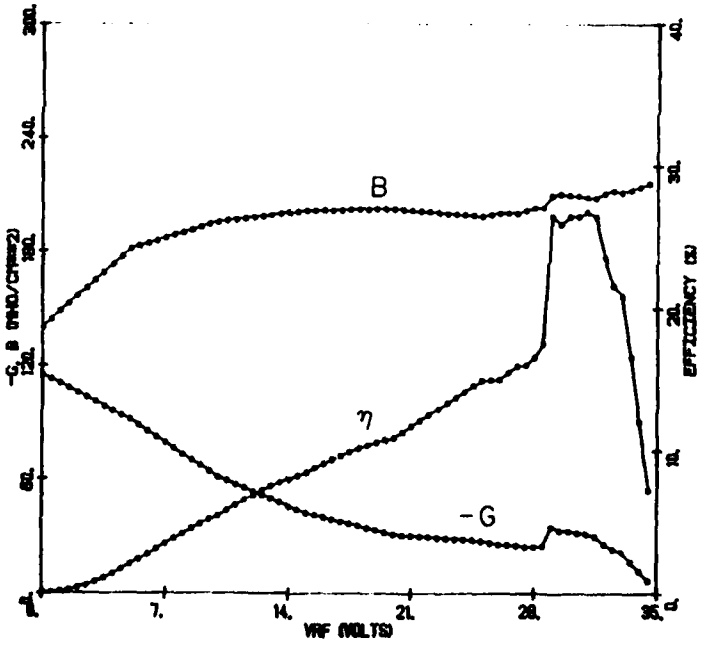

(b)

FIG. 4 LARGE-SIGNAL DATA FOR J_{dc} = 1250 A/cm^2.

(a) T = 400°K AND (b) T = 500°K.

T = 400°K in Figure 4a and T = 500°K in Figure 4b. It is seen that the range of V_{RF} for which simulations are carried out varies significantly with temperature; this fact complicates the interpolation process. Imagine, for example, that at some point in the simulation the program requires knowledge of $G(V_{RF} = 30\ V, J_{dc} = 1250\ A/cm^2, T = 450°K)$. One might be inclined at first to simply average the values of G at $V_{RF} = 30$ V in the curves of Figure 4. However, it is seen in Figure 4a that in order to obtain a value of G at $V_{RF} = 30$ V the last values simulated must be extrapolated, and since the $-G(V_{RF})$ curve has a large negative slope at the upper end of the V_{RF} range, the value obtained for $G(T = 400°K, V_{RF} = 30\ V)$ will be very large and positive. This value will be much larger than the relatively small negative conductance $G(T = 500°K, V_{RF} = 30\ V)$ obtained from Figure 4b and it will dominate the average. Therefore, for V_{RF} greater than 22.5 V (the largest value in Figure 4a), the extrapolated conductance curve in Figure 4a will dominate until the temperature becomes very close to 500°K. However, this is not the expected behavior; the value of V_{RF} for which $G(V_{RF},T) \cong 0$ is expected to vary gradually from $V_{RF} = 22.5$ V to $V_{RF} = 35$ V as T varies from 400°K to 500°K. This interpolation scheme does not give the expected behavior because it assumes linear variation in a region which is highly nonlinear.

Figure 5 illustrates the interpolation scheme used to circumvent this problem. The quantity $G(V,T_i)$ is desired, where results are known for T = 400°K and T = 500°K and where $400 \leq T_i \leq 500$. If RATIO denotes the quotient of RF voltage ranges that were simulated at the known temperatures,

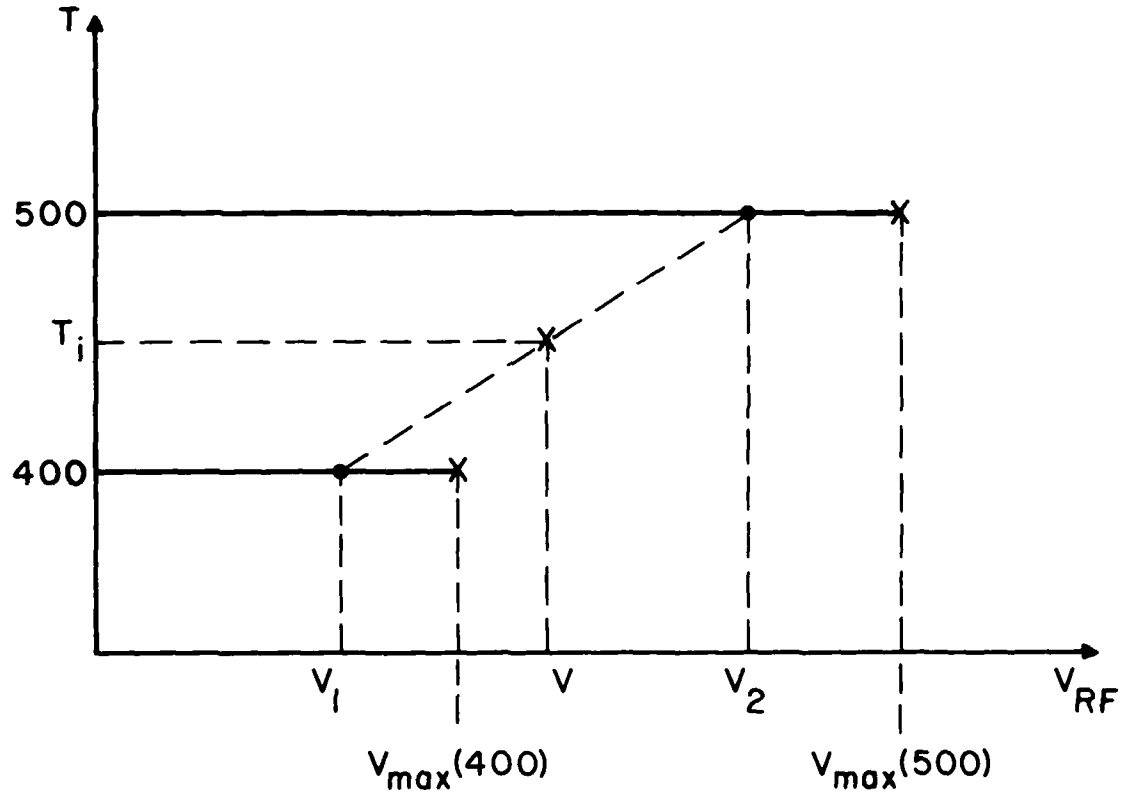

FIG. 5 ILLUSTRATION OF THE INTERPOLATION METHOD BETWEEN TWO TEMPERATURES.

$$\text{RATIO} = \frac{V_{max}(500)}{V_{max}(400)} \quad , \tag{5}$$

and if TFACT denotes the fractional temperature interpolation,

$$\text{TFACT} = \frac{T_i - 400}{500 - 400} \quad . \tag{6}$$

Then V_1 and V_2 are determined such that:

$$\frac{V_2}{V_1} = \text{RATIO}$$

and

$$V_1 + \text{TFACT}(V_2 - V_1) = V \quad . \tag{7}$$

The interpolated value is then determined from

$$G(V,T_i) = G(V_1,400) + \text{TFACT}[G(V_2,500) - G(V_1,400)] \quad . \tag{8}$$

In this manner, a much more reasonable variation of G(V) with temperature is obtained. [If $V_1 > V_{max}(400)$ or $V_2 > V_{max}(500)$ in Figure 5, the same equations are used but extrapolated values of G are used in the final interpolation in Equation 8.] Variation of $B(V_{RF})$ and $V_{dc}(V_{RF})$ with temperature are calculated in the same way as for $G(V_{RF})$. Also, interpolation between different values of J_{dc} where T is a constant are handled by the same method; for that case the vertical axis in Figure 5 would represent J_{dc} instead of T.

The diode temperature T is allowed to vary as the simulation progresses. The equation governing this variation is assumed to be

$$\frac{dT}{dt} + \frac{T - T_A}{\tau} = \frac{R_{TH} P_D}{\tau} \quad , \tag{9}$$

where T_A is the ambient temperature (°K), R_{TH} is the diode thermal resistance (°K/W), P_D is the average dissipated power in the device (W), and τ is the thermal time constant (s). For the X-band GaAs device studied in this report, τ was assumed to be 1.5 μs based on the results of Olson.[4] The dissipated power is found from

$$P_D = \text{AREA}\left(V_{dc}J_{dc} + \frac{V_{RF}^2}{2} G_D\right) , \qquad (10)$$

where AREA is in cm^2, J_{dc} is in A/cm^2 and G_D is in $mhos/cm^2$.

If P_D is assumed constant during the time interval t_1 to t_2, the temperature at the end of the interval is given by

$$T(t_2) = [T(t_1) - T_A - R_{TH}P_D]e^{-(t_2-t_1)/\tau} + T_A + R_{TH}P_D . \qquad (11)$$

The dc current density in the device is assumed to start from zero at the beginning of the simulation and increase linearly until it reaches a constant maximum value. Similarly, at the end of the simulation J_{dc} decreases linearly from the maximum value to zero. In the simulations presented in this report, both the linear rise and fall times were chosen to be 1 ns.

The Overall Simulation Procedure

This section describes the method used to carry out the entire device-circuit interaction; references are made to specific portions of the program that were described in the preceding sections.

Figure 6a shows the RF circuit configuration. $I_\ell(\omega_o)$ is a sinusoidal injection current source used to investigate the pulsed-locked oscillator-amplifier case; it is set to zero to look at the

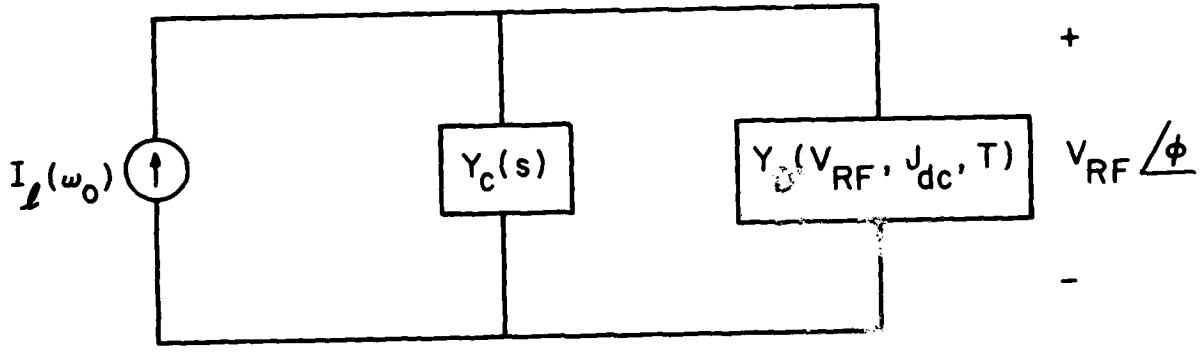

(a)

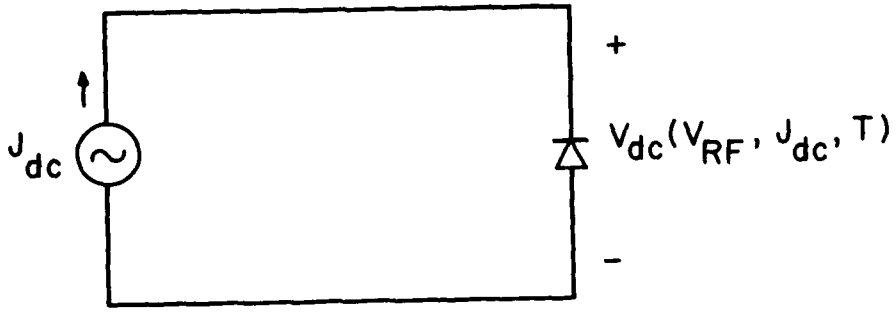

(b)

FIG. 6 (a) RF CIRCUIT AND (b) BIAS CIRCUIT USED IN THE SIMULATION.

free-running oscillator case. $Y_c(s)$ is the circuit admittance which varies with the complex frequency s; this is the input admittance of the circuit of Figure 2. $Y_D(V_{RF},J_{dc},T)$ is the large-signal diode admittance, which was determined for many combinations of V_{RF}, J_{dc} and T by running a finite-difference, large-signal program as described in the previous section. The simulated values are stored in tables and intermediate values of Y_D are found by the interpolation procedure described with reference to Figure 5.

Figure 6b shows the bias circuit consisting of a current generator with linear rise and fall times. A more complicated bias circuit could easily be included, however, this simple circuit was used for the preliminary investigations. V_{dc} of Figure 6b is the large-signal diode dc voltage; it was obtained, stored, and interpolated in the same manner as Y_D. In addition to the parameters shown in Figure 6, the temperature T varies according to Equation 9.

In Figure 6a, V_{RF} and ϕ are the amplitude and phase of the RF voltage across the device. As previously explained, these quantities are regarded as functions of time and are assumed to vary slowly with respect to the RF period. The time variation of these quantities is determined by solving Equations 3 and 4. To find the complex frequency $s = \sigma + j\omega$ to use in Equations 3 and 4, the following equation for the circuit of Figure 6a must be solved:

$$Y_c(s) + Y_D(V_{RF},J_{dc},T) = \frac{I_L}{V_{RF}} e^{-j\phi} \quad , \qquad (12)$$

where the only variable is s and all other parameters are considered locally constant. The admittance $Y_c(s)$ of the circuit in Figure 2 can be expressed as

$$Y_c(s) = \frac{P_3(s)}{P_4(s)} \quad , \tag{13}$$

where P_3 and P_4 are polynomials of the third and fourth order in s, respectively. The coefficients in these polynomials also depend on s since they include the factors tanh $(s\ell_1/c)$ and tanh $(s\ell_2/c)$, where ℓ_1 and ℓ_2 are the transmission-line lengths and c is the velocity of light. Using Equation 13, Equation 12 can be rewritten as

$$F(s) = P_3(s) + \left(G_D + jB_D - \frac{I_L}{V_{RF}} e^{-j\phi}\right) P_4(s) = 0 \quad . \tag{14}$$

To find the s value for which F(s) = 0, Newton's iteration method is used. The program starts with an initial guess for s. Next, F(s) and dF(s)/ds are calculated; in the dF(s)/ds calculation the s-dependence of the coefficients of the polynomials P_3 and P_4 must be considered so that the expression for this derivative is quite involved. Then, a better guess for s is obtained using the formula:

$$s_{new} = s - \frac{F(s)}{dF(s)/ds} \quad . \tag{15}$$

This iteration process is continued until the magnitude of F(s) is sufficiently small compared to the magnitudes of the individual terms in Equation 14.

For the case with a nonzero injection current I_L, an initialization procedure must be carried out before starting the simulation. It is assumed that between bias pulses $J_{dc} = 0$ but the injection signal is present as in Figure 6a. Therefore, a substantial RF voltage exists before the bias pulse is turned on, even though the diode is

passive. If the simulation were started with zero RF voltage, the circuit of Figure 6a would go through a complicated transient containing many natural frequencies until this RF voltage is reached. The quasi-static form for $V_{RF}(t)$ in Equation 1 is not adequate to describe this transient. Therefore, the steady-state value of V_{RF} and ϕ in Figure 6a that exists before the bias pulse is turned on must be determined, and the simulation must be started with these values. The equation which must be solved is

$$Y_c(j\omega_o) + Y_D(V_{RF}, T = T_o, J_{dc} = 0) = \frac{I_L}{V_{RF}} e^{-j\phi} , \qquad (16)$$

where ω_o is the frequency of the injection current source and T_o is the starting temperature. The procedure is to vary V_{RF} until the magnitudes of the left- and right-hand sides of Equation 16 are equal; then the phase ϕ is set so that the angle of the right-hand side equals that of the left-hand side. This procedure is carried out in a program called INITIAL.

Typically, all the parameters for the circuit of Figure 2 are known except for Z_1, the characteristic impedance of the quarter-wave transformer near the diode. Also, the large-signal characterization of the diode results in current and admittance per unit area, so that the diode area must be specified. The determination of Z_1 and diode AREA is simplified by noting that at the design frequency, ℓ_2 and ℓ_1 in Figure 2 are set to $\lambda/2$ and $\lambda/4$, respectively; therefore, the two transmission lines in series can be replaced by a single impedance inverter with constant $K = Z_1^2$. The problem then reduces to finding the proper K and AREA values. It is desired to match the diode-circuit combination at a particular frequency ω_o and for a particular

large-signal diode operating point, specified by $G_D + jB_D$ mho/cm^2 and V_{RF}. The equation to be solved is:

$$(G_D + jB_D)\ \text{AREA} + Y_c(j\omega_o, K) = \frac{I_L}{V_{RF}} e^{-j\phi} \quad , \qquad (17)$$

where the circuit admittance is a function of the as yet undetermined impedance inverter constant K. I_L and ϕ specify the desired injection vector at the operating point; I_L is zero for the free-running case. Since Equation 17 is a complex equation, it yields two equations which are sufficient to determine K and diode AREA for the desired operating point. This determination is carried out by the program DETKA.

Figure 7 presents a flow chart showing how the quasi-static simulation is carried out. Once the circuit parameters are determined except for Z_1 in Figure 2 and a diode operating point is chosen, the program DETKA is run to determine Z_1 and the diode area using Equation 17. Then if a nonzero injection signal is present, the starting V_{RF} and ϕ are determined by solving Equation 16 in the program INITIAL. For the free-running case, the RF voltage is started at 0.1 V, which is the smallest value the program allows V_{RF} to assume. (This is essentially the noise voltage which is assumed to exist, from which the oscillation builds up.) At this point the initialization is complete and the QS program is run, which carries out the time evolution of the solution. The linear turn-on of J_{dc} is started; the large-signal diode admittance and dc voltage are interpolated for the new J_{dc} using the procedure outlined in Figure 5; the new complex frequency s is determined in subroutine SOLVE which solves Equation 12 using a Newton iteration; after s is known, V_{RF} and ϕ are updated using Equations 3 and 4; after determining the new V_{RF}, a new diode dissipated power

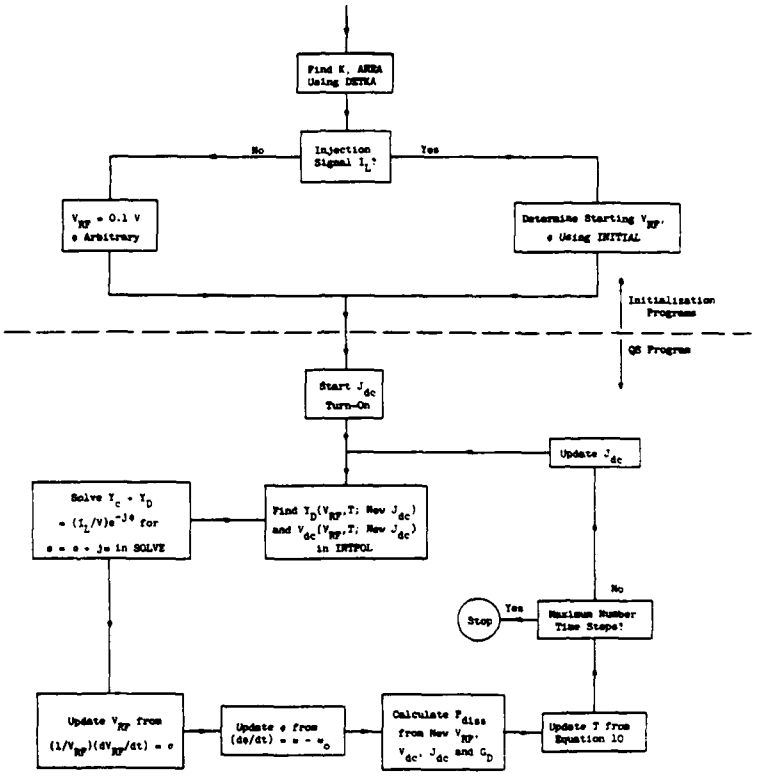

FIG. 7 FLOW CHART OF QUASI-STATIC SIMULATION.

P_{diss} is calculated according to Equation 10; the temperature T is updated from Equation 11; and finally the cycle is completed by updating J_{dc} another time step. (Of course J_{dc} reaches a constant value after the 1-ns rise time.) In practice, it is necessary to run the QS program at least three times for the entire simulation since different time steps are used during the turn-on period, the time for which J_{dc} is constant, and the turn-off period. Therefore the program is written so that it is easily restarted from a previous solution.

The update of temperature T involves the evaluation of an exponential as seen in Equation 11; however, since the time step is uniform throughout the simulation, this exponential need only be evaluated once. The solution of Equation 3 for the V_{RF} update is:

$$V_{RF}(t_2) = V_{RF}(t_1)e^{\sigma(t_2-t_1)} , \qquad (18)$$

so that the exponential must be evaluated at every time step since σ is changing. This is carried out by the function EXPO(x) in the QS program, which evaluates the standard series expansion for e^x and retains the number of terms in the series sufficient to give 1-percent accuracy.

Simulation Results Using a High-Low GaAs IMPATT and a 10-μs Bias Pulse

In this section simulation results are presented both for the free-running oscillator case and for the case with an injection signal present. For the free-running case, the component values used for the circuit of Figure 2 as well as the diode characteristics at the steady-state operating point are given in Table 1. Zl and diode AREA were determined in DETKA as was explained in the previous section,

Table 1

Diode and Circuit Parameters for the Free-Running Oscillator Case

Circuit Parameters

RL = 500 Ω	ℓ_2 = 1.5 cm	L_s = 0.24 nH
C = 6.422 pF	Z_2 = 50 Ω	R_s = 0.25 Ω
L = 0.0396 nH	ℓ_1 = 0.75 cm	I_L = 0
R = 50 Ω	Z_1 = 33.9 Ω	
	C_p = 0.32 pF	

Diode Parameters at Steady-State Operating Point

J_{dc} = 1250 A/cm^2 , V_{dc} = 44.6 V , V_{RF} = 30 V , f = 10 GHz

G_D = - 32.85 mho/cm^2 , B_D = 210 mho/cm^2

R_{TH} = 17.38°K/W , AREA = 2.809 x 10^{-4} cm^2 , T = 500°K

Equation 17. The parallel resonant circuit modeling the cavity was tuned to 9.98 GHz, which allows the oscillation to build up at a lower temperature than if the resonance is tuned to 10 GHz, the operating frequency.

Figure 8 shows a plot of the negative of the circuit admittance vs. frequency, together with the small-signal diode admittance vs. temperature, at $J_{dc} = 1250$ A/cm^2. Since, according to Equation 3, σ must be positive for V_{RF} to build up and since $\sigma < 0$ at the beginning of the simulation, V_{RF} cannot build up until $\sigma = 0$, which corresponds to the intersection of the two curves in Figure 8. When this intersection point is examined, it is concluded that the oscillation will not build up until the diode has heated up to almost 450°K. Also, the frequency of the RF voltage as the amplitude starts to build up will be approximately 10.27 GHz.

It should be noted in Figure 4b that the magnitude of the diode negative conductance is decreasing at the operating point of $V_{RF} = 30$ V. If an operating point was chosen where the negative conductance magnitude is increasing with V_{RF}, the operating point would be unstable.[5] This type of instability, which would occur even if the diode temperature remained constant, will be referred to as an electronic instability in this report.

The other type of instability that can occur is thermal instability. The criterion for thermal stability at an operating point is[6]

$$\frac{\partial}{\partial T}\left(R_{TH}P_{diss}\right)\Big|_{T_o} < 1 \quad , \tag{19}$$

where T_o is the operating point temperature. In this report the thermal resistance is assumed to be constant, so it may be removed from the

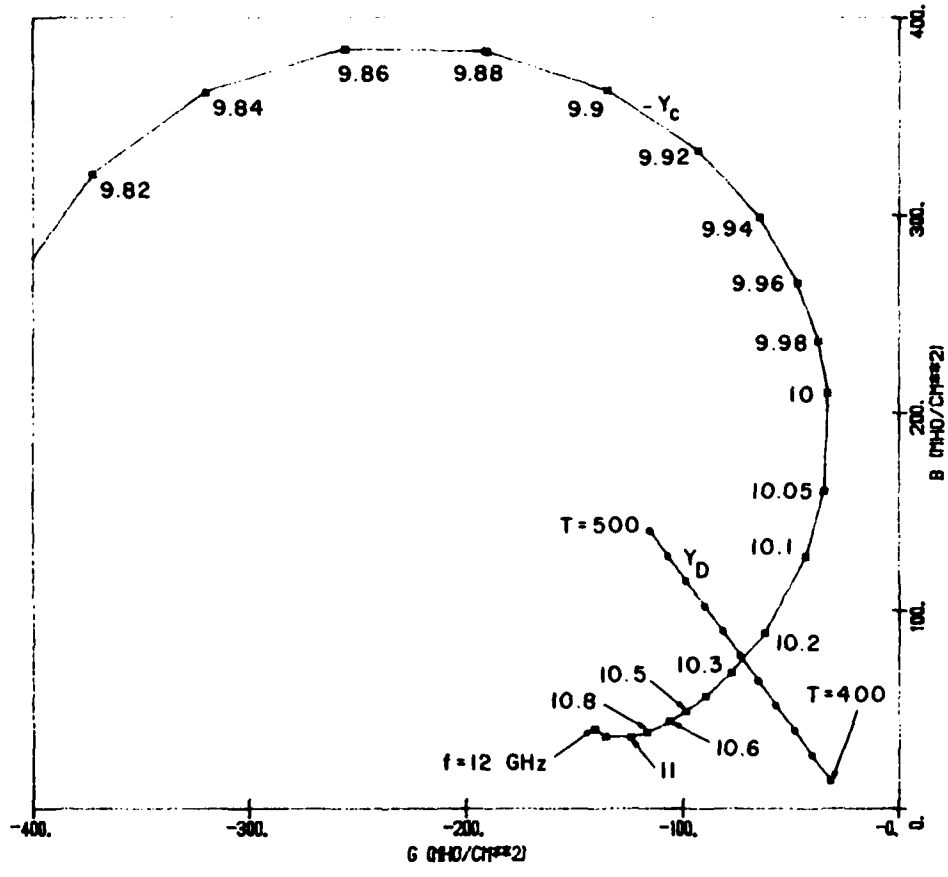

FIG. 8 CIRCUIT ADMITTANCE VS. FREQUENCY ($s = j\omega$) AND SMALL-SIGNAL DIODE ADMITTANCE VS. TEMPERATURE AT $J_{dc} = 1250\ A/cm^2$.

derivative in Equation 19. The procedure to check thermal stability is then to perturb the temperature to $T_o \pm \Delta T$, find the new operating point and thereby the new dissipated power P_{diss} at these temperatures, and finally calculate a finite difference approximation to Equation 19.

This procedure was carried out for the operating point at T_o = 500°K described in Table 1. If the temperature T is slightly below 500°K, the program interpolates between the large-signal diode characterizations stored at 400°K and 500°K; however, if T is slightly above 500°K, the program interpolates between values stored for 500°K and 535°K. Therefore, different results are expected depending upon whether the temperature is perturbed above or below 500°K. Perturbing the temperature from 500°K to 490°K yields the following result:

$$R_{TH} \cdot \frac{P_{diss}(T = 500) - P_{diss}(T = 490)}{10} = 0.39 \quad , \qquad (20)$$

so that thermal stability is assured if the temperature remains below 500°K. Calculating P_{diss} at 502°K gave the result:

$$R_{TH} \cdot \frac{P_{diss}(T = 502) - P_{diss}(T = 500)}{2} = 2.04 \quad , \qquad (21)$$

so that thermal runaway will occur if the temperature increases above 500°K.

Figure 9 shows the results for the free-running oscillator (I_L = 0). The time between pulses is many thermal time constants, so that the starting temperature was 300°K. The dc current was assumed to reach its maximum value at the first time step; for this case simulating the 1-ns ramp makes little difference since $\sigma < 0$ at the end of the pulse rise time. Figure 9b shows that the temperature reaches

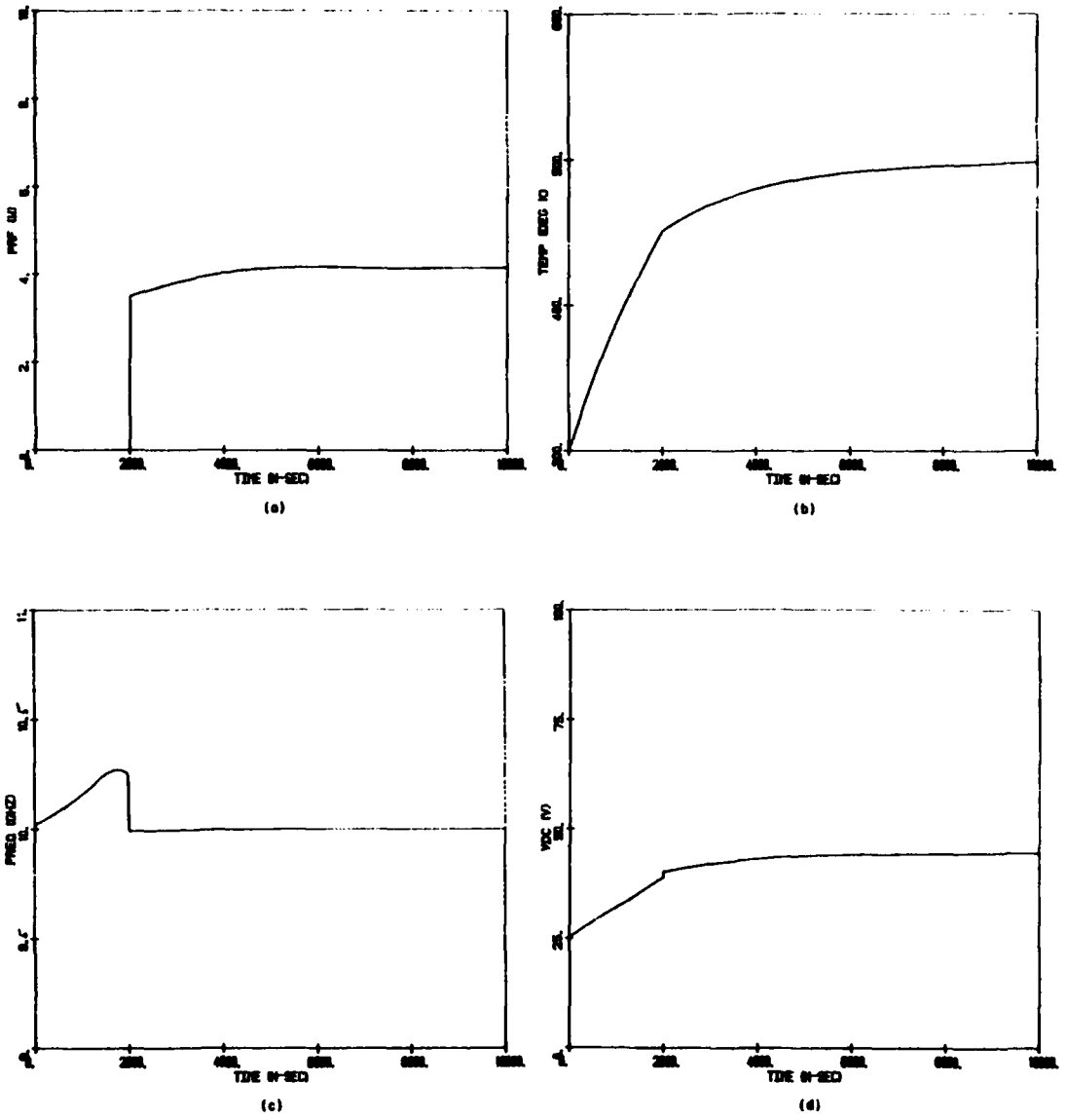

FIG. 9 (a) RF POWER, (b) TEMPERATURE, (c) FREQUENCY AND (d) DC VOLTAGE VS. TIME FOR THE FREE-RUNNING OSCILLATOR CASE.

approximately 450°K after 2 μs; based on Figure 8, the RF voltage is expected to build up at this point, which is confirmed by Figure 9a. (The time step used was 1 ns, so that although the RF power appears to turn on in one step, there are actually several time steps during the turn on.) After V_{RF} builds up, the dissipated power P_{diss} in the diode is reduced, since RF power is being generated; this causes the temperature to increase at a slower rate. Figure 9c shows that, again as expected from Figure 8, the frequency increases as V_{RF} builds up from small signal. After V_{RF} turns on, the frequency is nearly constant at 10 GHz. Figure 9d shows that a jump in the dc voltage occurs as V_{RF} builds up. (It was often observed in simulating nonpunch-through structures at constant temperature that V_{dc} increases with V_{RF} before decreasing near the point of maximum efficiency.) The dc voltage continues to increase slightly as the temperature increases, since the ionization rates are decreasing and therefore a higher field level is required to generate the same dc current.

Figure 10 shows the turn-off characteristics for this case. Note that the time scale is much smaller than for Figure 9. J_{dc} starts decreasing at t = 0 and reaches zero after 1 ns. It is seen that V_{RF} and P_{RF} decrease immediately, since the decrease is electronically dominated whereas the buildup in Figure 9 was thermally dominated. V_{dc} in Figure 10d decreases as J_{dc} decreases and the frequency in Figure 10c assumes a lower value as the diode admittance rapidly changes.

The temperature at the end of the simulation in Figure 9 was 498.2°K, so that thermal instability was not encountered. To test Equation 19, the simulation was restarted at a temperature of 502°K and thermal runaway did occur as predicted by Equations 19 and 21.

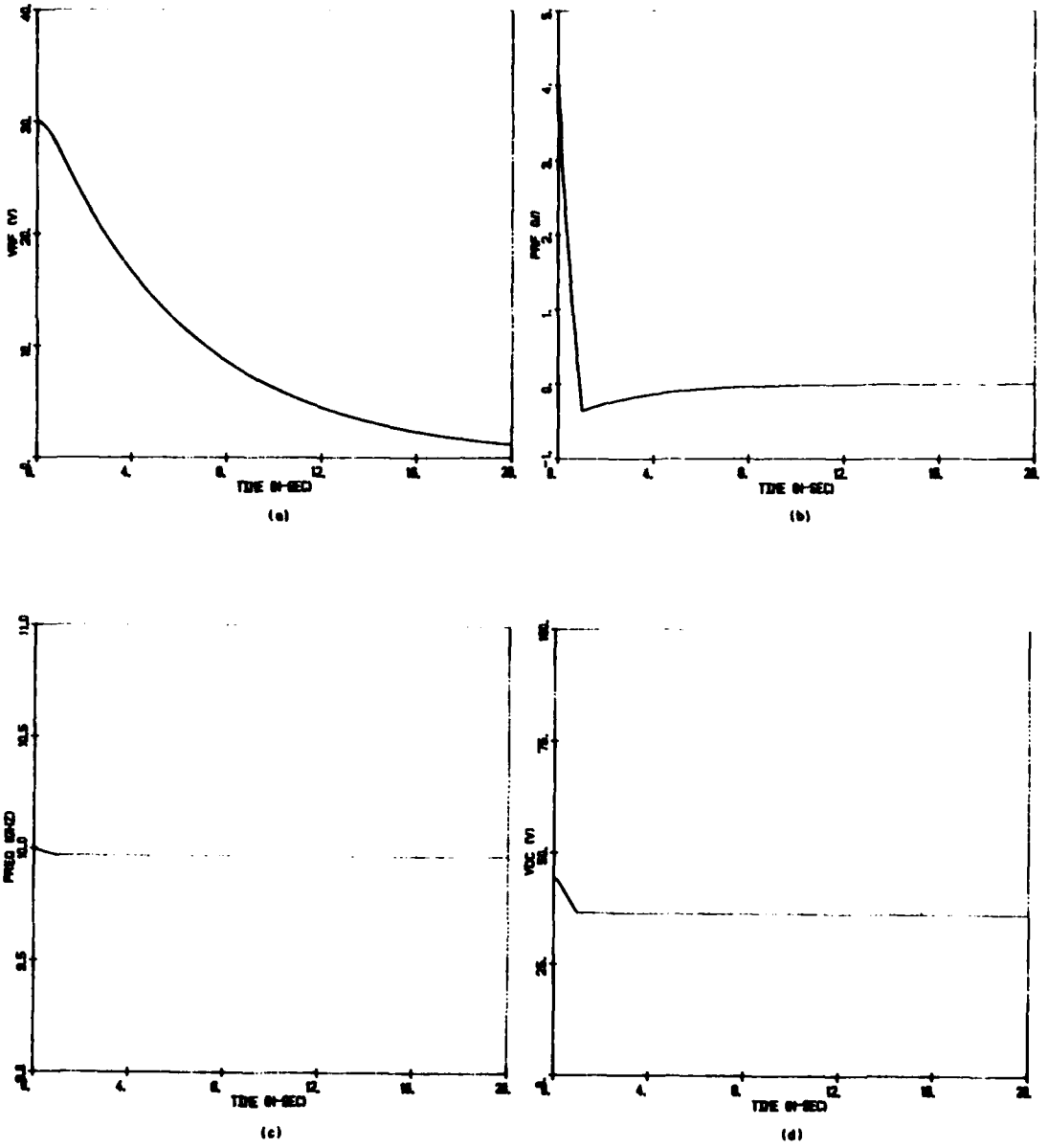

FIG. 10 (a) RF VOLTAGE, (b) RF POWER, (c) FREQUENCY AND (d) DC VOLTAGE DURING TURN-OFF FOR THE FREE-RUNNING CASE.

Next, the case with an injection signal present was investigated. Table 2 gives the parameters for this case. The injection current I_L was chosen so that the power from the injection source is approximately 10 dB down from the diode RF power at the steady-state operating point. This input power can be found approximately from:

$$P_i \approx \frac{I_\ell^2}{8 \cdot \mathrm{Re}\{Y_c\}} \quad . \tag{22}$$

The program DETKA was run to solve Equation 17 for K and AREA. Figure 11 shows a plot of the negative of the circuit admittance and the large-signal diode admittance vs. V_{RF} near the steady-state operating point. The two curves do not intersect at the operating point as for the free-running case, but rather the admittances are separated by the "injection vector" which is the right-hand side of Equation 17, shown as an arrow in Figure 11. This vector has zero angle since ϕ was chosen to be zero, and its magnitude is $I_L/(V_{RF} \cdot \mathrm{AREA}) = 0.16/(29 \times 2.512 \times 10^{-4})$ = 22 mho/cm^2. At the start of the simulation ($J_{dc} = 0$), the program INITIAL must be run to determine the initial steady-state amplitude and phase of the RF voltage. For this case it was found that $V_{RF} = 3.54$ V and $\phi = -1.2$ rad.

Figure 12 shows simulation results during the 1-ns rise time as J_{dc} increases linearly from zero to 1250 A/cm^2. In Figure 12a, V_{RF} starts from the value determined by the INITIAL program. Because a substantial V_{RF} exists across the diode at t = 0, the RF voltage can start building up immediately without the delayed start effect seen for the free-running case. Figure 12c shows that the frequency is greater than the steady-state operating value during the turn-on, which is expected since B_D for lower RF voltages is smaller and therefore

Table 2

Diode and Circuit Parameters for the Injection-Locked Case

Circuit Parameters

RL = 500 Ω	ℓ_2 = 1.5 cm	L_s = 0.24 nH
C = 6.422 pF	Z_2 = 50 Ω	R_s = 0.25 Ω
L = 0.0396 nH	ℓ_1 = 0.75 cm	I_L = 0.16 A
R = 50 Ω	Z_1 = 46.11 Ω	ϕ = 0
	C_p = 0.32 pF	

Diode Parameters at Steady-State Operating Point

J_{dc} = 1250 A/cm^2 , V_{dc} = 44.3 V , V_{RF} = 29 V , f = 10 GHz

G_d = - 34.93 mho/cm^2 , B_D = 209.9 mho/cm^2

R_{TH} = 19.57°K/W , AREA = 2.512 x 10^{-4} cm^2 , T = 500°K

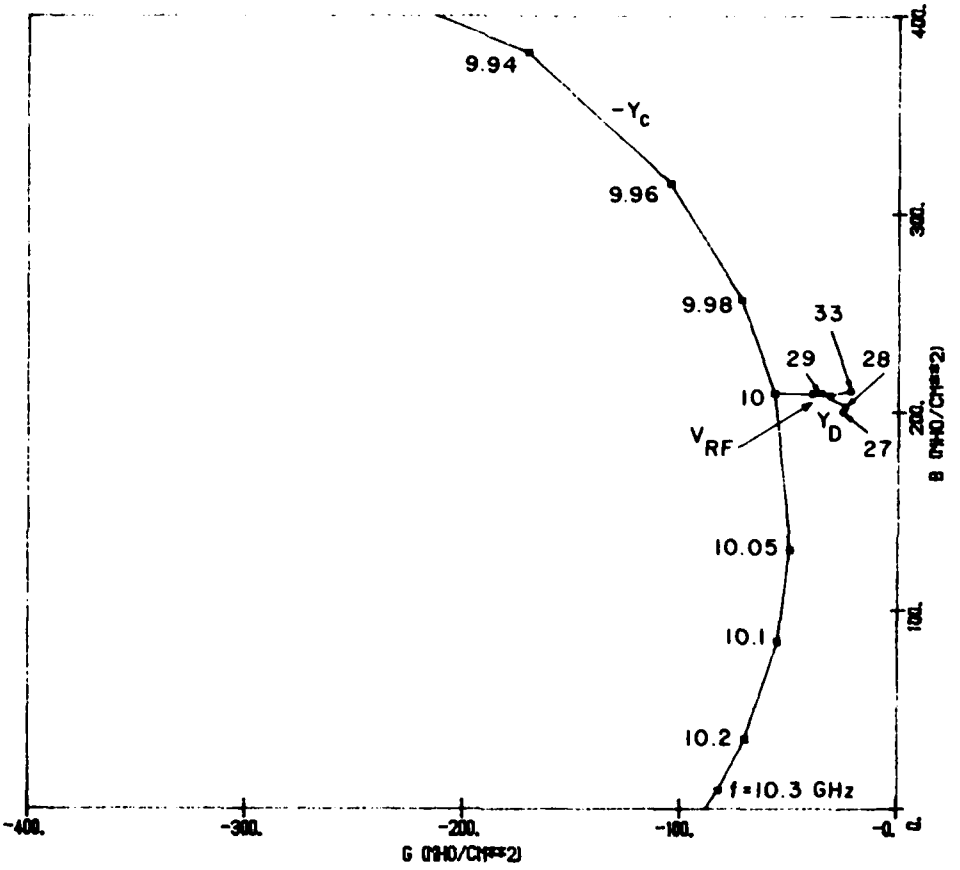

FIG. 11 NEGATIVE CIRCUIT ADMITTANCE VS. FREQUENCY AND DIODE ADMITTANCE VS. V_{RF} AT T = 500°K AND J_{dc} = 1250 A/cm².

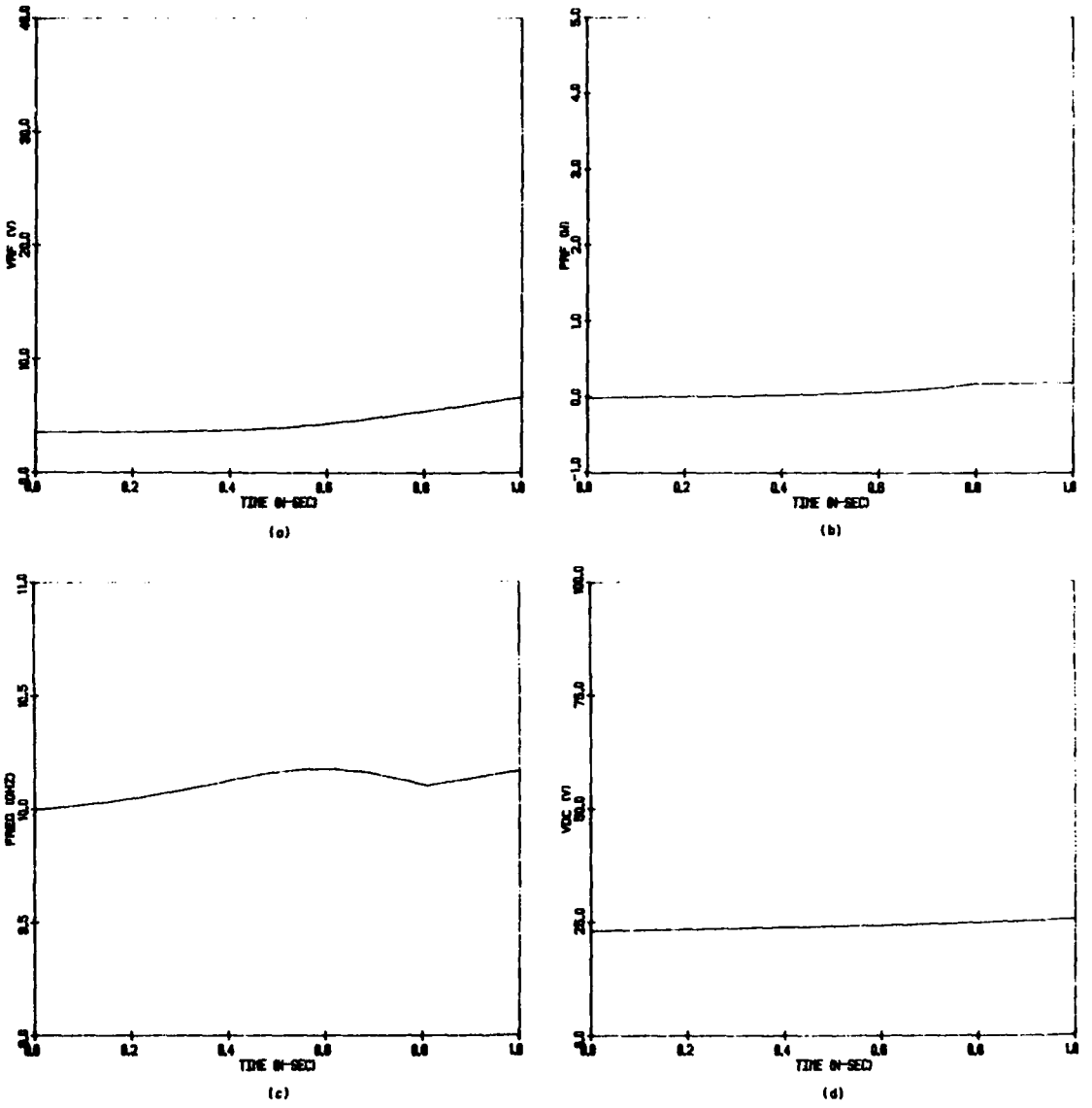

FIG. 12 (a) RF VOLTAGE, (b) RF POWER, (c) FREQUENCY AND (d) DC VOLTAGE DURING THE 1-ns PULSE RISE TIME FOR THE INJECTION-LOCKED CASE.

the Y_D curve of Figure 11 moves down into the portion of $-Y_c(f)$ corresponding to higher frequencies.

Figure 13 shows results starting just as J_{dc} reaches its constant maximum value and continuing for 1 μs. For this portion of the simulation it was necessary to use Δt = 0.1 ns rather than 1 ns as for the free-running case; therefore, this 10-μs simulation was performed in steps. The gradual increase of V_{RF} in Figure 13a is due to the gradual temperature rise shown in Figure 13c. Note that because the delayed start effect does not occur, the temperature rises more slowly than for the free-running case in Figure 9, since the diode dissipated power is lower. The frequency rapidly reaches the steady-state value, as shown in Figure 13b.

Figures 14a and c show that the RF voltage and temperature continue to gradually rise during the 1- to 2-μs period. The frequency is very close to 10 GHz as is seen in Figure 14b.

Figure 15 shows results for the remainder of the pulse width, from 2 to 10 μs. For this portion a time step of Δt = 1 ns could be used, since the parameters were not changing as rapidly with time as for the earlier portions. Figure 15a shows that the RF voltage reaches the steady-state value late in the pulse width. The frequency remains at 10 GHz, as is seen in Figure 15b. From Figure 15c it is seen that the diode does not reach the steady-state temperature until near the end of the pulse. (Since the temperature never crosses 500°K, the thermal instability problem discussed previously is not encountered.) Figure 15d shows that the dc voltage gradually increases to the steady-state value of 44.3 V.

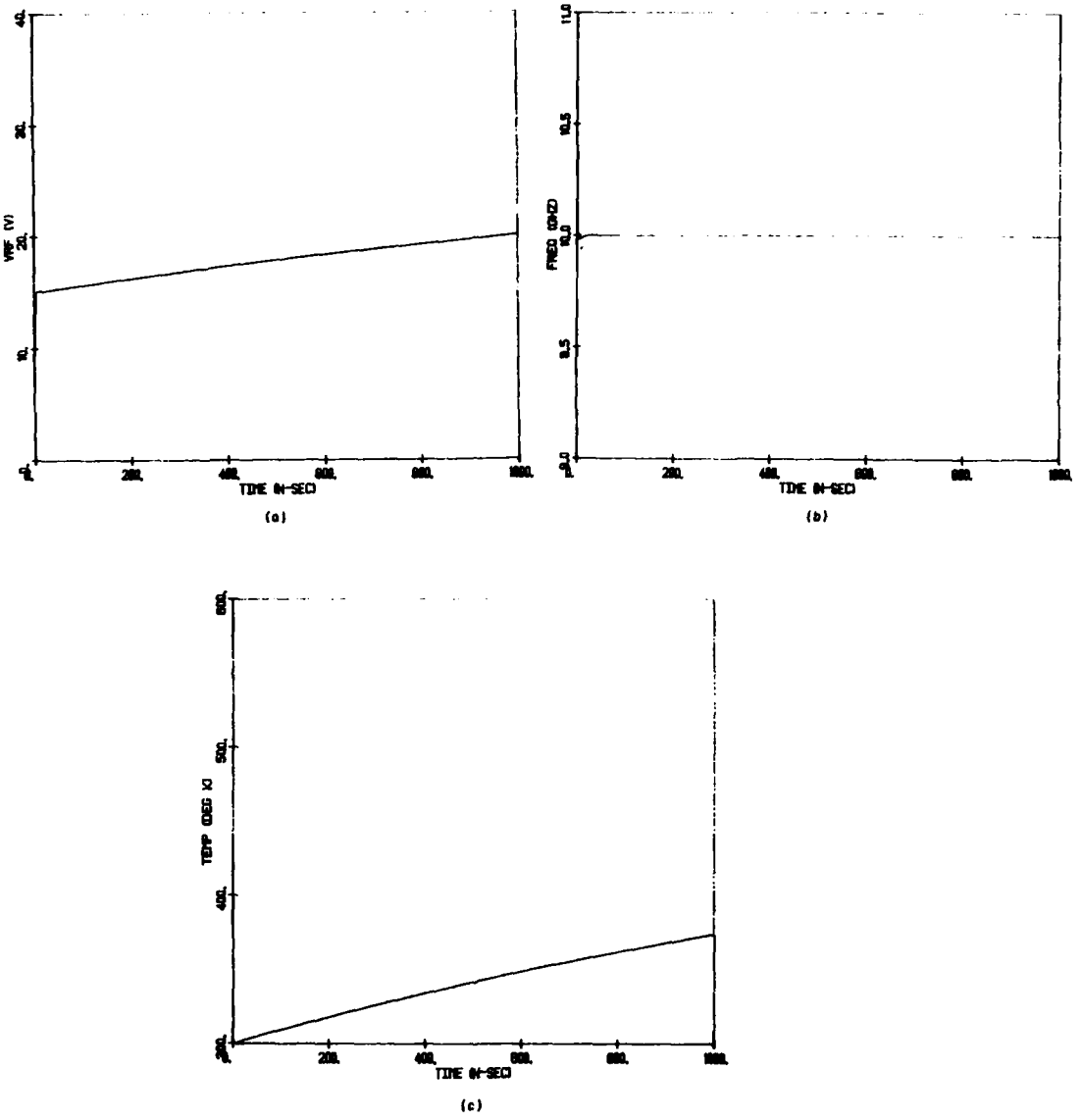

FIG. 13 (a) RF VOLTAGE, (b) FREQUENCY AND (c) TEMPERATURE FOR 1 ns AFTER BIAS PULSE TURN-ON FOR THE INJECTION-LOCKED CASE.

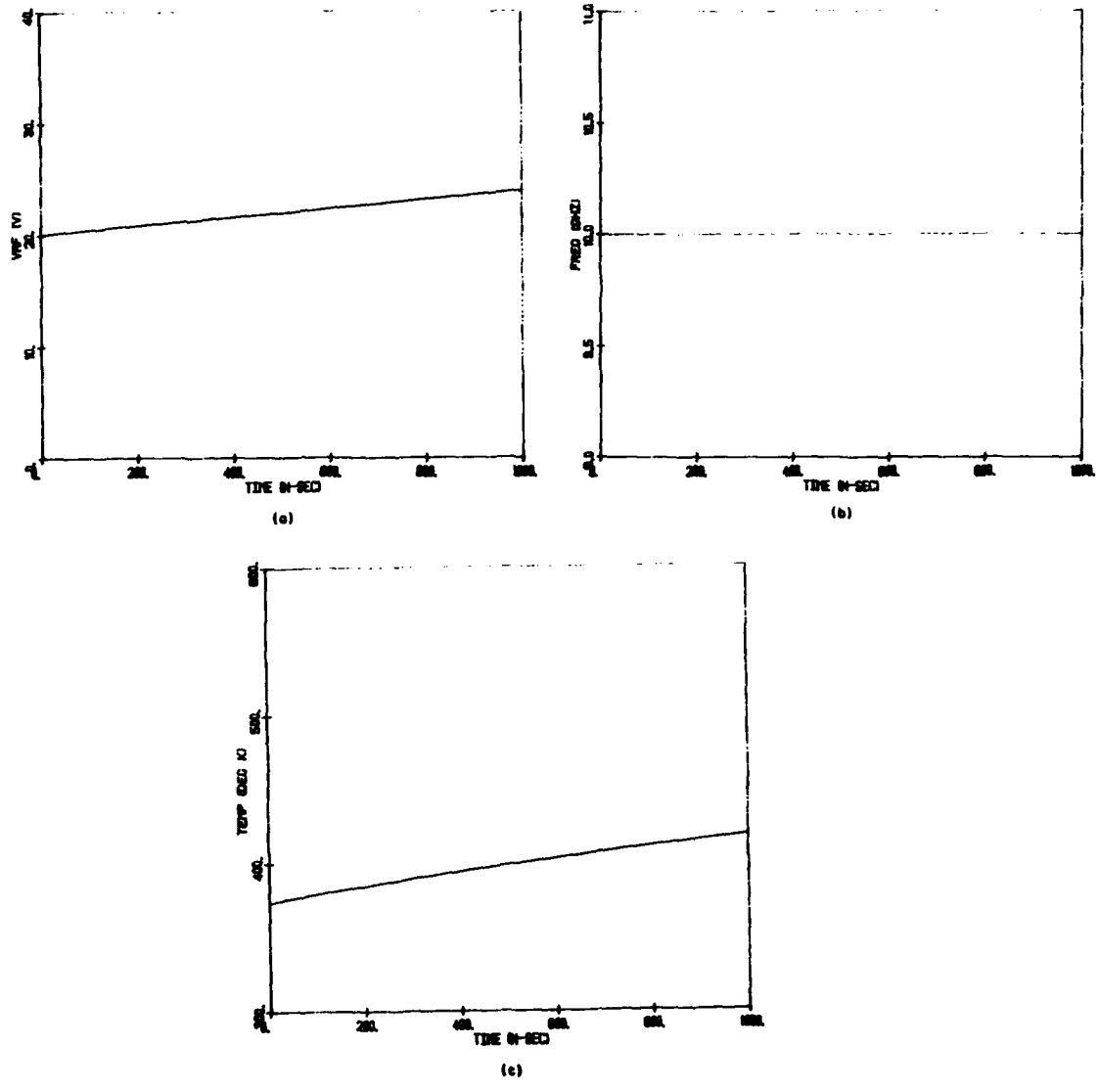

FIG. 14 (a) RF VOLTAGE, (b) FREQUENCY AND (c) TEMPERATURE DURING THE 1- TO 2-μs PERIOD FOR THE INJECTION-LOCKED CASE.

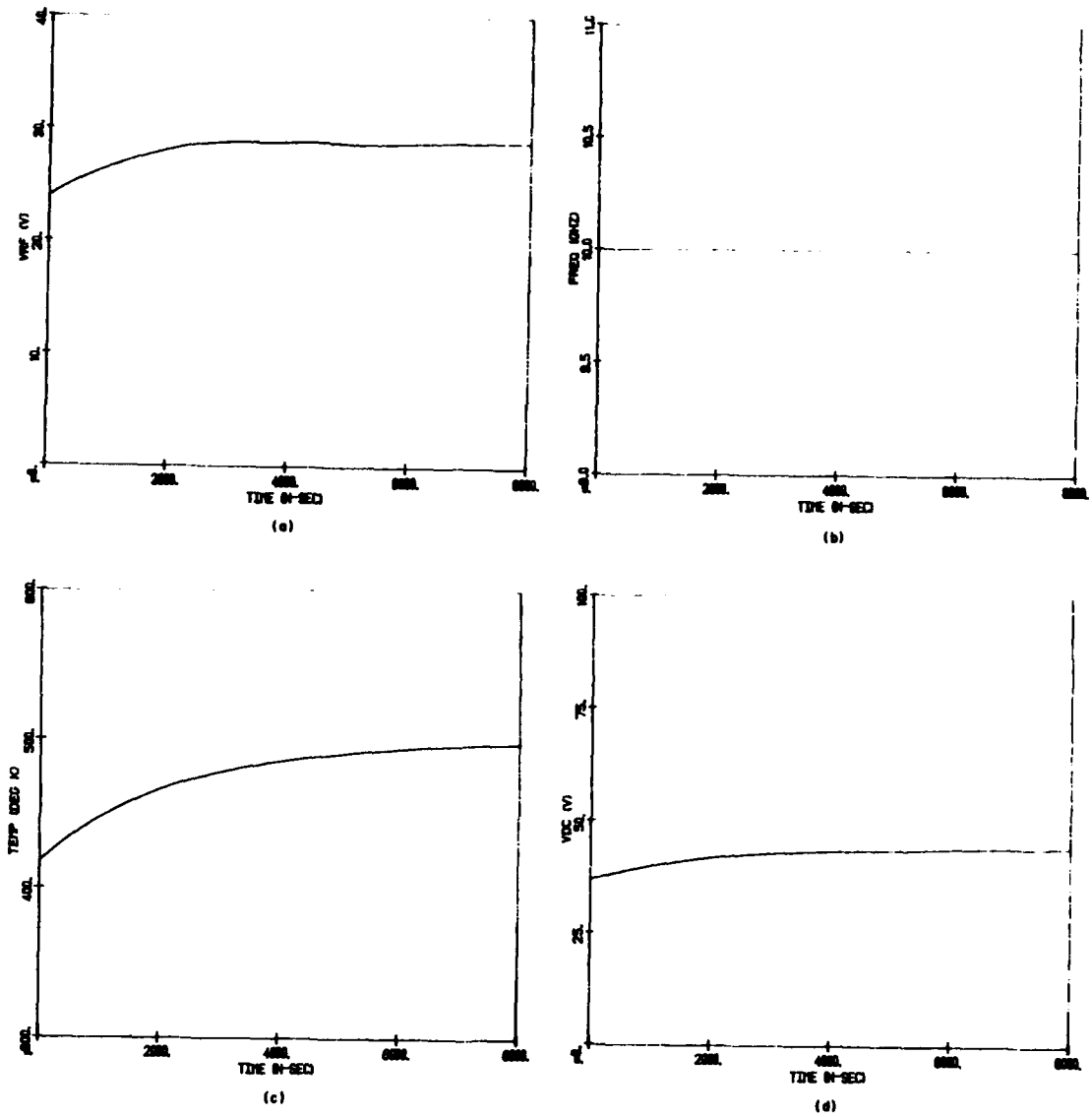

FIG. 15 (a) RF VOLTAGE, (b) FREQUENCY, (c) TEMPERATURE AND (d) DC VOLTAGE FROM 2 TO 10 μs FOR THE INJECTION-LOCKED CASE.

Figure 16 shows the turn-off characteristics as the bias current falls to zero during 1 ns. As for the free-running case, V_{RF} and P_{RF} in Figures 16a and b decrease rapidly due to electronic effects (the temperature is essentially constant throughout the 40-ns period). Again, the frequency in Figure 16c jumps to a lower value as the dc current decreases. There is a jump in dc voltage in Figure 16d, also due to the rapid decrease of J_{dc}.

Conclusions and Suggestions for Further Investigations

The quasi-static program is seen to be a useful tool in studying the dynamics of pulsed operation. Once the diode characterization is completed, the simulations are relatively inexpensive (a 10-μs simulation costs under $10).

There are many additional facets of pulsed operation that can be investigated using this program. One is the question of how the IMPATT diode operates under pulsed conditions when the dc current and pulse width are varied for a given diode-circuit combination. For the simulations in this report, the starting temperature was 300°K. However, as the time between pulses is reduced, the starting temperature begins to increase. Use of the quasi-static program in an iterative scheme would allow the determination of a consistent starting temperature.

Another important study would be the effect of different IMPATT doping profiles on pulsed operation. For example, low-high-low single-drift and various double-drift structures could be used. There is probably a significant difference also between operation using punch-through and nonpunch-through devices in each category. All of these effects are presently being studied.

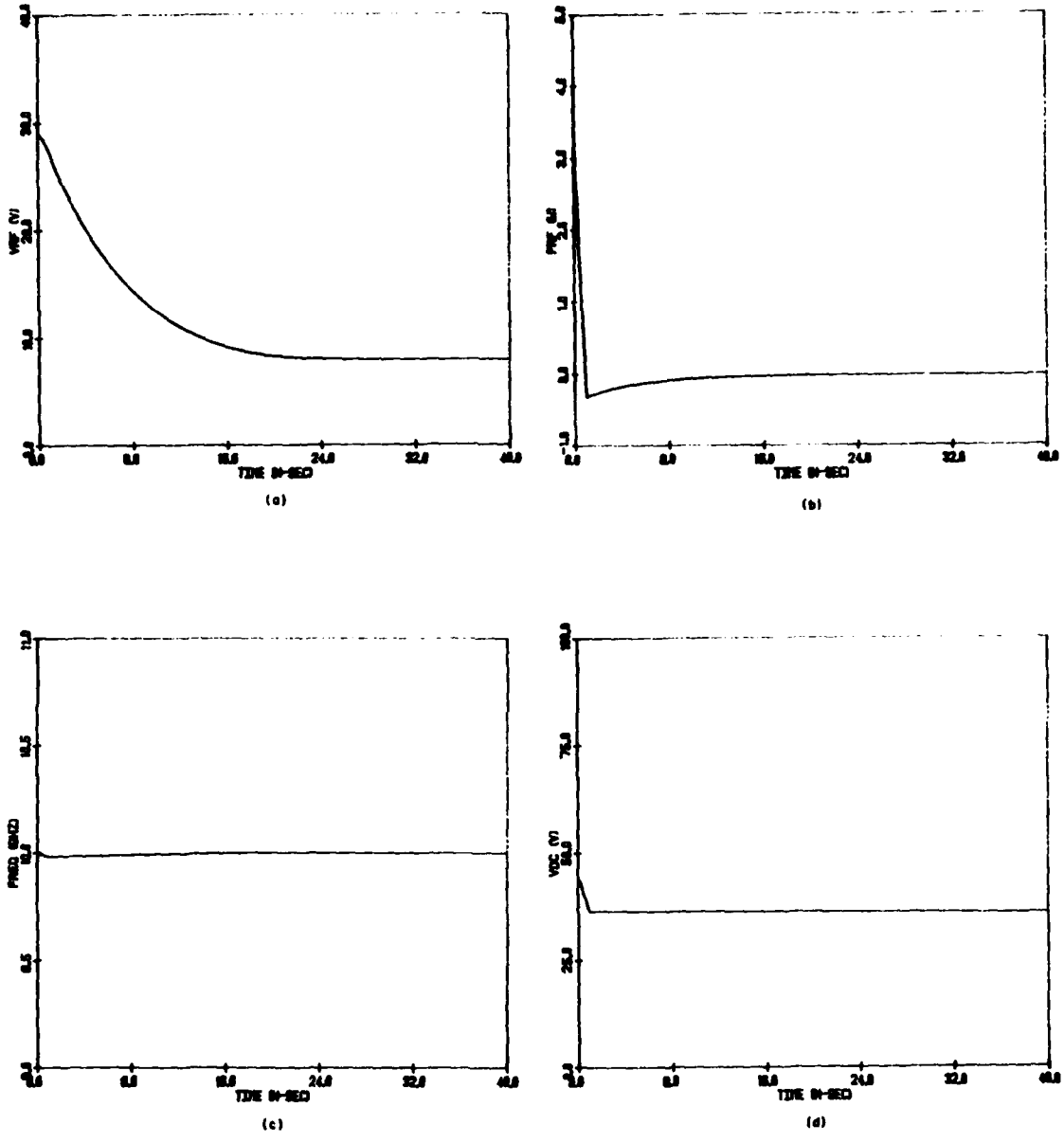

FIG. 16 (a) RF VOLTAGE, (b) RF POWER, (c) FREQUENCY AND (d) DC VOLTAGE AS J_{dc} DECREASES TO ZERO IN 1 ns FOR THE INJECTION-LOCKED CASE.

LIST OF REFERENCES

1. Kurokawa, K., "Injection Locking of Microwave Solid-State Oscillators," Proc. IEEE, vol. 61, No. 10, pp. 1386-1410, October 1973.

2. Russell, K. J., "Microwave Power Combining Techniques," IEEE Trans. on Microwave Theory and Techniques, vol. MTT-27, No. 5, pp. 472-478, May 1979.

3. Mains, R. K. and Haddad, G. I., "Properties of High-Efficiency X-Band GaAs IMPATT Diodes," Tech. Report No. AFWAL-TR-81-1066, Electron Physics Laboratory, The University of Michigan, Ann Arbor, January 1981.

4. Olson, H. M., "Temperature Transients in IMPATT Diodes," IEEE Trans. on Electron Devices, vol. ED-23, No. 5, pp. 494-503, May 1976.

5. Kurokawa, K., "Noise in Synchronized Oscillators," IEEE Trans. on Microwave Theory and Techniques, vol. MTT-16, No. 4, pp. 234-240, April 1968.

6. Grondin, R. O., Private communication.

*U.S.Government Printing Office: 1981 — 559-004/3008


DATE
IL ME